Supporting Information

Nanoscale Surface-Induced Unfolding of Single Fibronectin Is Restricted by Serum Albumin Crowding

Lauren A. Warning,[1] *Qingfeng Zhang,*[1,2] *Rashad Baiyasi,*[3]

*Christy F. Landes,** [1,2,3,4] *Stephan Link** [1,2,3]

[1]Department of Chemistry, [2]Smalley Curl Institute, [3]Department of Electrical and Computer Engineering, [4]Department of Chemical & Biomolecular Engineering, 6100 Main Street, Rice University, Houston, TX, 77005 USA

*Corresponding Authors: cflandes@rice.edu; slink@rice.edu

CONTENTS

1. Experimental methods

1a. Fn conjugation and characterization

Labeling reaction. The protocol was adapted from previous work[1] and performed at ambient temperature. Alexa 546 maleimide targets four possible free cysteine residues on FnIII-7 and FnIII-15 modules (Figure S1A). Equal volumes (600 µL) of 1 mg/mL human Fn in phosphate buffered saline (PBS, 20 mM phosphate, 150 mM NaCl) and 8 M guanidine hydrochloride (Sigma Aldrich) were combined, gently mixed, and let to sit for 5 min. Alexa 546 C_5 maleimide (1 mM, 125 µL) was added in 50-fold excess to Fn, and the reaction vessel was gently mixed during 2 hr incubation. Gravity size-exclusion chromatography was performed with a PD-10 desalting column using PBS as the equilibrium buffer to collect the purified Fn-546. The purification procedure followed a modified version of GE Healthcare's Instructions 52-1308-00 BB, in which 1-mL of Fn-546 was collected during the 2nd mL of elution collection. Purification removes excess free dye and guanidine hydrochloride from Fn-546.[2] Collected Fn-546 was stored in 1 µM aliquots for later use.

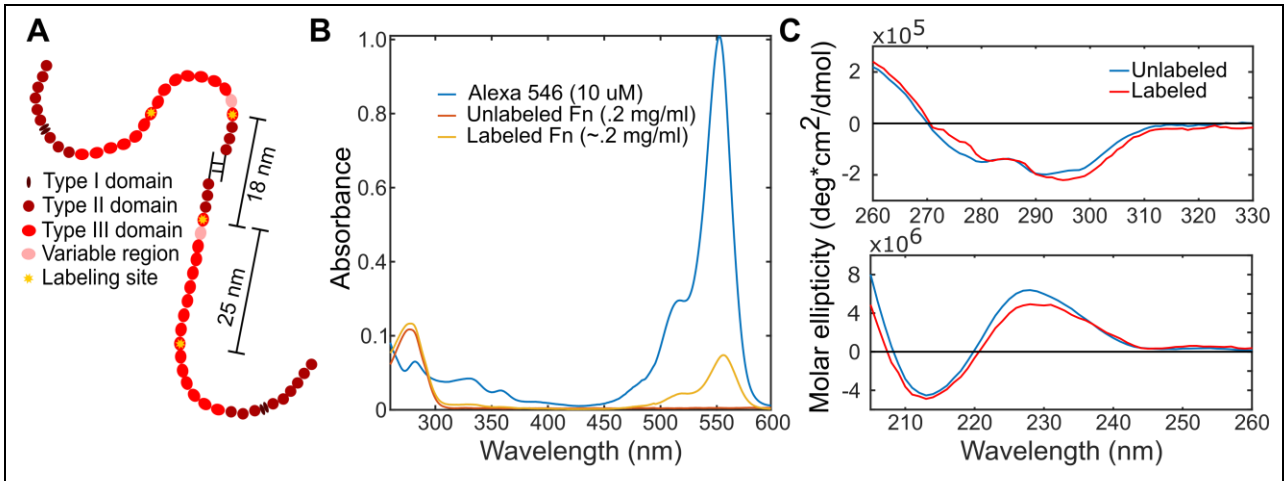

Figure S1. Characterization of Fn-546. (A) Illustration of Fn's multi-domain structure and labeling site positions. (B) Absorbance spectra used to quantify the degree-of-labeling. (C) Circular dichroism (CD) spectra of labeled and unlabeled Fn in the near and far UV regions.

Fn-546 characterization. Circular dichroism (CD) and absorbance measurements were performed for Fn-546 purity and structure analysis using a J-815 JASCO CD spectrometer with Peltier temperature control to 20 +/- 1 ^{o}C, at a scan speed of 200 nm/min with a bandwidth of 1.00 nm and averaged over 4 scans. Absorbance spectra collected in a 1 cm quartz cuvette were used to verify successful separation of Fn-546 and free dye and to calculate the degree of labeling. During Fn-546 purification trials, 0.5 mL aliquots of elutant were collected from size-exclusion chromatography. Absorbance measurements at 280 nm and 553 nm, indicators for Fn and Alexa 546 presence respectively, revealed that Fn-546 eluted during the 2nd milliliter, while most free Alexa 546 maleimide eluted at the 6th milliliter. Guanidine hydrochloride eluted after Alexa 546 given its smaller size. Successful Fn conjugation was confirmed as illustrated in Figure S1B. Degree of labeling (3-4 dyes/Fn) was calculated via Beer's law; extinction coefficients were calculated based on absorbance spectra collected for Alexa 546 maleimide and unlabeled Fn of known concentration in the exact buffer used for experiments. CD spectra of Fn confirmed that tertiary (260-330, 1 cm quartz cuvette) and secondary (205-260 nm, 1 mm quartz cuvette) structure were not significantly altered by the labeling process (Figure S1C).

1b. Single-molecule sample preparation

Coverslip cleaning. Coverslips were sonicated for 15 min in water/detergent and 15 min in acetone. After copious washing in deionized water, the coverslips were immersed in a basic piranha bath (6:1:1 water, 30% hydrogen peroxide, ammonium hydroxide) for 5 min at 70 ^{o}C. The slides were then washed with Millipore water and dried with nitrogen. Dried slides were cleaned for 2 min under oxygen plasma (PDC-32G; Harrick Plasma; medium power). Plasma-cleaned slides were submerged in Vectabond-acetone solution (2% vol/vol, Vector Laboratories,

Burlingame, CA) for 5 min, and then dipped into Millipore water to quench the aminosilanization reaction. Slides were dried under mild nitrogen flow and used immediately.

Protein solution details. Fn-546 aliquots were thawed at 37 ^{o}C for 10-15 min before their use. For experiments including HSA, a fresh 50 mg/mL solution was prepared in PBS from the dry solid for each sample preparation. Fn-only samples were prepared with 2.5 pM Fn-546 in PBS. Fn+HSA samples were prepared by mixing 10-100 pM Fn-546 with 7.5-45 mg/mL unlabeled HSA prior to exposure to the functionalized glass surface. For Fn-then-HSA experiments, 5 pM Fn-546 incubation was followed by 45 mg/mL HSA incubation. Higher amounts of Fn-546 were necessary to achieve the same surface density when mixed with higher concentrations of HSA because there are more HSA competing for the same surface area. However, we did find that the Fn-546 concentration necessary to achieve optimal Fn-546 density in Fn+HSA mixtures varied day-by-day on average by 14 pM, which is the result of working with picomolar concentrations, prone to dilution error. Additionally, proteins tend to adsorb to container surfaces. Although we minimized the time that thawed Fn-546 solutions spent in LoBind microcentrifuge tubes for multiple dilutions, Fn-546 adsorption to storage container walls becomes significant at picomolar concentrations and influences the effective concentration that is actually exposed to the sample surface.

1c. Microscope measurements

Photobleaching is minimized prior to data acquisition. Several precautions were performed in order to minimize dye photobleaching prior to actual single-molecule high resolution imaging with photobleaching (SHRImP) measurements. Before being placed on the microscope, all samples were prepared under low light conditions and completely protected from

light when not actively being used. Once on the microscope, each measured region was manually put into focus with excitation light passing through a 1.3x optical density filter. The filter decreased laser irradiation such that enough photons were still present for focusing but the rate of photobleaching was reduced. Even if some emitters photobleached prior to the start of the measurement, we still could acquire adequate single Fn-546 intensity traces, because only 2 emitters out of the 3-4 emitters per Fn-546 were needed for SHRImP analysis.

Positional error due to stage drift is negligible. Stage drift was determined to be negligible under the experimental conditions performed. Samples were secured to a piezoelectric stage that held x and y-positions constant throughout the video. However, focus drift can still occur, particularly immediately after an image is put into focus. In order to minimize drift, the sample was left to sit for at least 45 seconds prior to data acquisition. After this waiting period, over the entire 1000 frame video (10 s) the image drift was <1 pixel (64 nm). SHRImP analysis considered periods of up to 48 frames, and therefore the error due to drift over this period of time would be <3.2 nm. This error is smaller than our theoretical photon-limited localization precision of 7 nm and is therefore considered negligible for this experiment.

2. Analysis

2a. DNA rulers

To test the accuracy and precision of our SHRImP method, we measured surface-adsorbed Alexa 546-dually-labeled duplex DNA rulers of known length (8- and 30-nm). Duplex DNA rulers labeled with Alexa 546 at their 5' ends were obtained from Integrated DNA Technologies. The 8-nm ruler was 24-bp in length (CGGTCCTATCGGATTCTGGGTCCT and complement) and the 30-nm ruler had 89-bp (TAGTATTAGACGACATTATCACCTTAGCGT

TACATCGGAGCAGACCTACAGATAGACATCCAGACGAGGCTACATTGCGATTCCAC TAT and complement). DNA samples were prepared similarly to protein samples and adsorbed to aminosilanized glass from a 15 pM solution. Higher illumination intensity was used for DNA experiments; intensity was reduced for Fn-546 experiments in order to resolve the increased number of photobleaching steps (four steps for Fn-546 versus two steps for DNA).

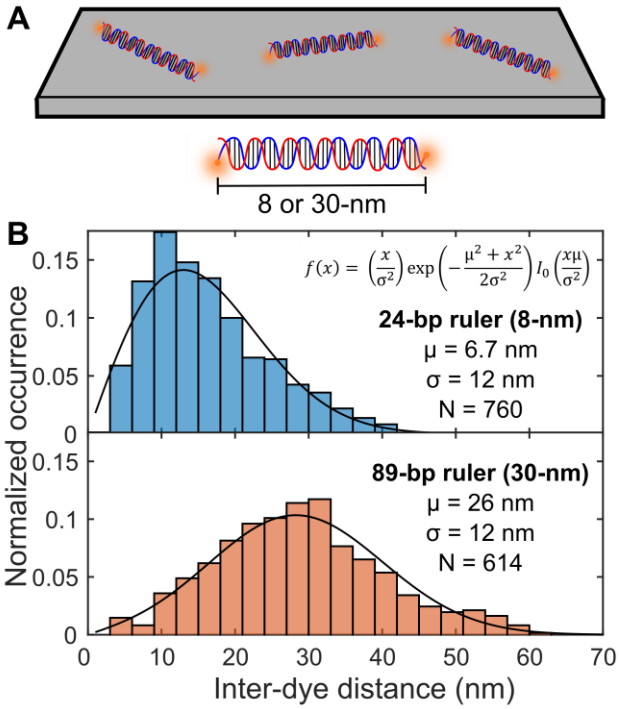

Figure S2. SHRImP resolution quantification with DNA rulers. (A) Representation of DNA rulers of known length (8 or 30-nm) adsorbed to aminosilanized glass. (B) Experimentally measured inter-dye distances for each ruler length. Data were fitted with a non-normal distribution equation for inter-dye distances,[3] given as an inset in top panel, where μ is the true inter-dye distance, σ is the distance measurement's standard deviation, and I_0 is the modified Bessel function of integer order zero.

We fitted the SHRImP-determined distances to a non-normal distribution that describes inter-dye distances in fluorescence localization techniques (Figure S2).[3]

$$\textbf{Equation 1}: \quad f(x) = \left(\frac{x}{\sigma^2}\right) \exp\left(-\frac{\mu^2+x^2}{2\sigma^2}\right) I_0\left(\frac{x\mu}{\sigma^2}\right)$$

In this equation, μ is the true inter-dye distance, σ is the standard deviation of the distance measurement, and I_0 is the modified Bessel function of integer order zero.[3] From the parameters in Equation 1, we can experimentally determine DNA ruler length (μ) and SHRImP precision (σ). Data points were filtered as discussed in the main text. Additionally, <6% of data points were removed as outliers for Equation 1's fit if they were larger than 1.5 times the inter-quartile distance from the median of the dataset. DNA ruler lengths were only a few nanometers smaller than the true length: the 8-nm ruler was 6.7 nm, and the 30-nm ruler was 26 nm. The underestimation could be explained by the DNA rulers not lying perfectly flat on the aminosilanized glass surface. Both ruler distributions produced a SHRImP precision of 12 nm. Individual emitter localization precision is related to distance measurement precision with the following equation: $\sigma_{emitter}{}^2 + \sigma_{emitter}{}^2 = \sigma_{inter-emitter\ distance}{}^2$. Therefore, experimental localization precision for a single emitter is 12 nm / $\sqrt{2}$ = 8 nm. These results are close to our predicted localization precision of 7 nm based on photon counts.[4]

Other groups reported similar or better precision with DNA samples, but several of these studies used Gaussian or lognormal fits to the inter-dye distance distributions to assess accuracy and precision.[5-6] Such fits are prone to systematic errors and can therefore misrepresent the accuracy and precision of the measurement.[3] The alternative non-Gaussian fit that we applied in the current work is more appropriate.[3] Dye choice also varied among published results and could influence the measured values. Cyanine dyes (e.g. Cy3) are frequently used on DNA due to their well-understood stability for this system,[5-7] but these dyes are destabilized as protein conjugates;

Alexa dyes like Alexa 546 exhibit better fluorescence as protein conjugates.[8] We used Alexa 546 on both our DNA controls and Fn-546 for consistency.

2b. Analysis approach for Fn-546

Because Fn-546 exhibited larger variations in measured inter-dye distances than the control DNA samples, Fn-546 data required different analysis strategies. The fit employed for the DNA rulers is appropriate because there is a single true inter-dye distance. Adsorbed Fn-546 is expected to exhibit many possible inter-dye distances due to variation in label location and, more importantly, heterogeneous Fn-546 conformations. Labeling of Fn's cysteine residues is random,[7] and because Fn-546 from the same batch was used for all experiments, labeling position heterogeneity is consistent sample-to-sample. Previous single-molecule measurements showed that surface-adsorbed Fn exhibits many possible conformations.[7, 9-10] Therefore, when comparing Fn-546 distance distributions for different conditions of crowding, we considered differences in the range of conformations that are possible, rather than strict conformational states. All data points that passed the data filtration steps described in the main text were considered.

Distance distributions are represented as averaged histograms and complementary cumulative distribution functions to account for variation from multiple trials, and statistical significance was further quantified with the K-S comparison for non-normal data. Triplicate experiments were performed to capture any trial-to-trial variation in inter-dye distributions. The averaged histograms (Figures 2 & S4) were generated as follows: We produced single trial histograms by discretizing SHRImP-determined distances into 5 nm bins. Because N was not exactly the same for each trial, we normalized each histogram to illustrate the fraction of each

bin's occurrence within the single trial's sample population. We then produced averaged histograms by averaging the fractional occurrence value of each 5 nm bin among the triplicate experimental data sets. In Figures 2-3, the same data is represented as averaged complementary cumulative distribution functions (CCDFs) with standard deviation derived from the three trials. Averaged cumulative distributions have previously been used by theoreticians to compare polyglutamine conformation.[11] We executed K-S two-sample comparisons for non-normal data using the averaged CCDFs to assess the statistical significance of differences between the tested conditions.

2c. Discussion of individual trials

Figure S3 depicts the individual trials of Fn-546 distance distributions in varying conditions with HSA as CCDFs; these distributions were averaged in the main text figures, because we observed reproducible trends among these trials. The first set of experiments (A-C) tested Fn-546's unfolding when co-adsorbed with varying amounts of HSA. The K-S comparison for non-normal data distinguishes Trial 3's Fn-only distribution from the HSA-containing distributions ($p < 0.05$). While the K-S test does not distinguish distributions in Trials 1 and 2, qualitatively assessment confirms that in the individual trials unrestricted Fn-546 exhibits higher occurrence of large inter-dye distances. The second set of experiments (D-F) tested Fn-546's unfolding without HSA (Fn-only), coadsorbed with 45 mg/mL HSA (Fn+HSA), and sequentially exposed to 45 mg/mL HSA (Fn-then-HSA). We observed that Fn-only always exhibits the greatest fractions of increased unfolding, Fn+HSA exhibits the least, and Fn-then-HSA is in the middle. When the K-S test is used in Trials 1 and 2, the distributions are indistinguishable from each

other ($p > 0.05$). In Trial 3, Fn-only and Fn-then-HSA are indistinguishable by the K-S test ($p > 0.05$), but Fn+HSA is distinguishable from both Fn-only and Fn-then-HSA ($p < 0.05$).

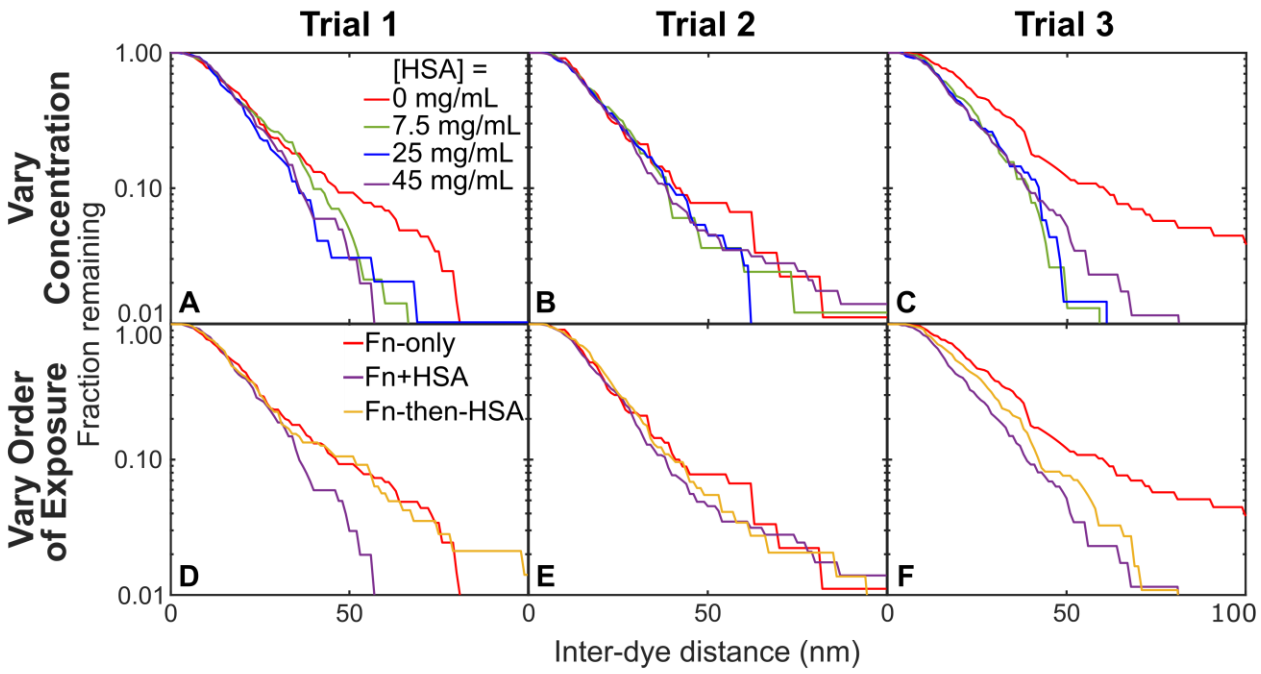

Figure S3: Triplicate SHRImP experiments reveal consistent trends. The data shown in Figures 2 and 3 of the main text are generated from these triplicated results. Data sets were assigned to Trial 1, 2, and 3 based on order of the experiment's data collection. (A-C) Inter-dye distance distributions for Fn-546 co-adsorbed with varying concentrations of HSA. (D-F) Inter-dye distance distributions for Fn-only, co-adsorbed with HSA (Fn+HSA), and Fn-546 with sequential HSA exposure (Fn-then-HSA).

2d. Additional discussion of averaged trials

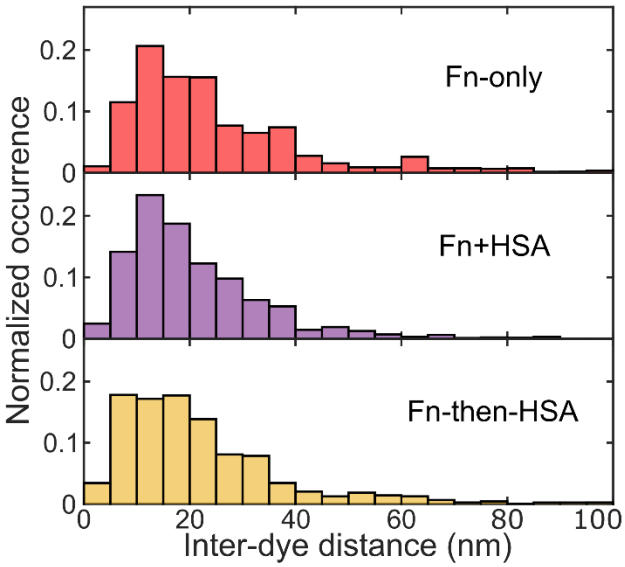

Figure S4: HSA introduction after initial Fn-546 adsorption does not alter Fn-546's conformation as effectively as co-adsorbed HSA. Histogram representation of the data presented in Figure 3. Averaged histogram distributions of triplicate SHRImP-determined inter-dye distances of single surface-adsorbed Fn-546 under conditions with no HSA (Fn-only), coadsorption with HSA (Fn+HSA), and sequential exposure to HSA (Fn-then-HSA).

The K-S test results in Table S1 correspond to the averaged data distributions depicted in Figures 2, 3, and S4. According to K-S test results, the Fn-only distribution is distinguishable from all conditions with co-adsorbed HSA. Fn-546's unfolding when sequentially exposed to HSA (Fn-then-HSA) is more similar to Fn-only than to Fn-546 coadsorbed with HSA (Fn+HSA). The K-S test distinguishes Fn-only and Fn+HSA, but not Fn-only and Fn-then-HSA. However, the corresponding *p*-value to the latter, 0.053, is much smaller than the *p*-value associated with Fn-only compared to Fn-then-HSA, 0.245.

Table S1: K-S comparison of Fn-546 inter-dye distances with varying HSA conditions.

Table S1 summarizes K-S test *p*-values when comparing the specified distributions by averaging the triplicate distributions.

Compare by [HSA] (mg/mL)		*P-value*	*Distinguishable with 95% confidence? ($p < 0.05$)*
0	7.5	0.039	Yes
0	25	0.019	Yes
0	45	0.000	Yes
7.5	25	0.392	No
7.5	45	0.407	No
25	45	0.839	No
Compare by order of exposure			
Fn-only	Fn+HSA	0.000	Yes
Fn-only	Fn-then-HSA	0.245	No
Fn+HSA	Fn-then-HSA	0.053	No

The observed inter-dye distances in Figure 2 are expected to vary partially due to a heterogeneous distribution of possible conformations or subpopulations.[7, 10, 12] It is possible that only a fraction of Fn-546—those that are the most unfolded—are affected by the HSA crowding. Fn-546 in both the crowded and uncrowded cases exhibit many conformations of inter-dye distances equal to or less than 10-15 nm (the mode of the histograms), and this fact could be due to subpopulations of Fn-546 conformations that are common to both the crowded and uncrowded conditions. However, it is also possible that a larger fraction of Fn-546 exhibit restriction in unfolding with HSA crowding, but is hidden by variation in dye position, heterogeneity in Fn-546 conformation, and localization precision.

REFERENCES

1. Smith, M. L.; Gourdon, D.; Little, W. C.; Kubow, K. E.; Eguiluz, R. A.; Luna-Morris, S.; Vogel, V., Force-induced Unfolding of Fibronectin in the Extracellular Matrix of Living Cells. *PLoS Biol.* **2007,** *5* (10), e268.

2. Antia, M.; Islas, L. D.; Boness, D. A.; Baneyx, G.; Vogel, V., Single Molecule Fluorescence Studies of Surface-Adsorbed Fibronectin. *Biomaterials* **2006,** *27* (5), 679-90.

3. Churchman, L. S.; Flyvbjerg, H.; Spudich, J. A., A non-Gaussian distribution quantifies distances measured with fluorescence localization techniques. *Biophys. J.* **2006,** *90* (2), 668-71.

4. Thompson, R. E.; Larson, D. R.; Webb, W. W., Precise Nanometer Localization Analysis for Individual Fluorescent Probes. *Biophys. J.* **2002,** *82* (5), 2775-2783.

5. Gordon, M. P.; Ha, T.; Selvin, P. R., Single-molecule High-resolution Imaging with Photobleaching. *Proc. Natl. Acad. Sci. U. S. A.* **2004,** *101* (17), 6462-5.

6. Qu, X.; Wu, D.; Mets, L.; Scherer, N. F., Nanometer-localized Multiple Single-molecule Fluorescence Microscopy. *Proc. Natl. Acad. Sci. U. S. A.* **2004,** *101* (31), 11298-303.

7. Klotzsch, E.; Schoen, I.; Ries, J.; Renn, A.; Sandoghdar, V.; Vogel, V., Conformational Distribution of Surface-adsorbed Fibronectin Molecules Explored by Single Molecule Localization Microscopy. *Biomater. Sci.* **2014,** *2* (6), 883.

8. Panchuk-Voloshina, N.; Haugland, R. P.; Bishop-Stewart, J.; Bhalgat, M. K.; Millard, P. J.; Mao, F.; Leung, W.; Haugland, R. P., Alexa Dyes, a Series of New Fluorescent Dyes that Yield Exceptionally Bright, Photostable Conjugates. *Journal of Histochemistry & Cytochemistry* **1999,** *47* (9), 1179-1188.

9. Bergkvist, M.; Carlsson, J.; Oscarsson, S., Surface-dependent Conformations of Human Plasma Fibronectin Adsorbed to Silica, Mica, and Hydrophobic Surfaces, Studied with Use of Atomic Force Microscopy. *J. Biomed. Mater. Res. A* **2003,** *64A* (2), 349-356.

10. Erickson, H. P.; Carrell, N. A., Fibronectin in Extended and Compact Conformations. Electron Microscopy and Sedimentation Analysis. *J. Biol. Chem.* **1983,** *258* (23), 14539-14544.

11. Vitalis, A.; Wang, X.; Pappu, R. V., Atomistic simulations of the effects of polyglutamine chain length and solvent quality on conformational equilibria and spontaneous homodimerization. *J. Mol. Biol.* **2008,** *384* (1), 279-97.

12. Johnson, K. J.; Sage, H.; Briscoe, G.; Erickson, H. P., The Compact Conformation of Fibronectin Is Determined by Intramolecular Ionic Interactions. *J. Biol. Chem.* **1999,** *274* (22), 15473-15479.